ELSEVIER

Journal of Structural Geology 29 (2007) 453–466

JOURNAL OF STRUCTURAL GEOLOGY

www.elsevier.com/locate/jsg

Strain refraction, viscosity ratio and multi-layer deformation: A mechanical approach

Kieran F. Mulchrone [a,*], Patrick A. Meere [b]

[a] *Department of Applied Mathematics, National University of Ireland, Cork, Ireland*
[b] *Department of Geology, National University of Ireland, Cork, Ireland*

Received 13 March 2006; received in revised form 17 October 2006; accepted 17 October 2006
Available online 30 November 2006

Abstract

A solution for the deformation of viscous layers during a two-dimensional general deformation is derived. Layer deformation is found to consist of components of pure shear, simple shear and pure rotation when considered with respect to the layer orientation. It is shown that for external bulk pure shear the layer deformation is typically vastly different to that outside the layer, ranging from pure to simple to super shear depending on layer orientation and viscosity contrast. Treagus' method for determining viscosity ratio from cleavage refraction is re-evaluated and is found to applicable under bulk pure shear. However, the presence of earlier LPS (layer-parallel shortening) can lead to erroneous viscosity ratio estimates. A new approach is developed, relying on the variation of cleavage orientation with layer orientation that is found to be robust with respect to LPS. The method is applied to examples from the Irish Variscides and the new approach has implications for determining whether or not LPS occurred in this foreland setting.

Keywords: Cleavage refraction; Viscosity ratio; Vorticity; Finite strain

1. Introduction

Cleavage refraction is a common feature in folded low-grade meta-sedimentary sequences where variations in bedding layer competencies lead to changes in the orientation and intensity of strain across these layers. The phenomenon was first described in detail by Sorby (1853) who, along with Harker (1886), believed it to represent refraction of finite strain where cleavage tracks the XY plane of the finite strain ellipsoid. This general relationship of finite strain to cleavage has and continues to cause considerable controversy. Field studies by Siddans (1972) and Wood (1974) clearly demonstrated that the cleavage plane in highly deformed slates corresponds to the XY plane of finite strain. The finite-element studies of Dietrich (1969), Dietrich and Carter (1969), and Shimamoto & Hara (1976) confirmed the view that cleavage planes are parallel to the XY plane. Treagus (1983) theoretically modelled refraction in planar Newtonian layers assuming a homogenous strain and a heterogenous simple shear component that predicted strong changes in strain ellipsoid shape, magnitude and orientation across viscosity contrasts. However, the assertion by Treagus (1988) that the relationship between strain and cleavage and consequently between strain refraction and cleavage refraction was not fully understood, is still valid today especially with strain/fabric development in more competent lithologies. Ramsay (1982) was the first to use the relationship of layer competence to cleavage refraction (cleavage refracting towards bedding in less competent layers) to work out an 'order of competence' in multilayers. Treagus (1999) went on, with some limitations, to numerically quantify this effect in multilayers.

Treagus (1999) considered the possibility of determining viscosity ratio using cleavage refraction. She concluded that, because cleavage orientations may be immeasurably close to the bedding normal (i.e. the direction initially normal to bedding and subsequently deformed), cleavage refraction patterns in rocks may provide a simple method of determining effective rock viscosity ratios. The method is based on the

* Corresponding author. Tel.: +353 21 4903411; fax: +353 21 4271040.
E-mail address: k.mulchrone@ucc.ie (K.F. Mulchrone).

0191-8141/$ - see front matter © 2006 Elsevier Ltd. All rights reserved.
doi:10.1016/j.jsg.2006.10.004

shear strain-rate ratio and more practically the shear strain ratio across a boundary being equal to the inverse viscosity ratio (Treagus, 1983, 1988, 1999). This rule emerged from considering the buckling instability of a layer oblique to the principal compression direction (Treagus, 1973). The unperturbed state requires stress refraction between layer and matrix for interfacial continuity. Treagus (1981) presented a 3D theory for stress and infinitesimal strain refraction in oblique layers indicating that strong variations in the orientation and shape of the infinitesimal strain ellipsoid may occur from layer to layer. Both Cobbold (1983) and Treagus (1983) derived the simple expression relating strain-rate ratio and viscosity ratio and Treagus (1983) further presented an algebraic relationship between finite strain refraction and viscosity ratio. Also, the finite strain may be factored from the strain refraction into a layer-normal pure shear and a layer-parallel simple shear (Treagus, 1988). Given this strain factorization, viscosity ratios are estimated from cleavage refraction (Treagus, 1999).

In this paper a different, dynamic approach to strain refraction is taken, based on the two-dimensional theoretical framework for the motion of a non-rigid ellipse immersed in a viscous fluid recently developed by Mulchrone and Walsh (2006). The evolution of cleavage refraction is described in context of a progressive deformation as bedding rotates during buckling.

2. Layer deformation

2.1. Single layer

Mulchrone and Walsh (2006) derived a solution for the motion of a viscous ellipse (long axis a and short axis b) immersed in a viscous fluid under a general deformation in 2D, where the ratio between the external and internal viscosities is given by μ_r. In addition, no slipping was allowed at the interface between the inclusion and the enclosing material. It was assumed that the fluids were Newtonian and that the flow was Stokes flow, in other words dominated by viscous effects and characterised by a low Reynolds number. By letting the long axis (a) of the ellipse approach infinity, the ellipse becomes a layer of infinite extent with across-layer thickness b. Therefore modifying the equations derived by Mulchrone and Walsh (2006) by taking the limit as $a \to \infty$, we find expressions governing the motion of an infinite layer under a general deformation.

The set of differential equations reduce to:

$$\frac{\mathrm{d}\phi}{\mathrm{d}t} = \frac{1}{2}(L_{21} - L_{12} + (L_{12} + L_{21})\cos 2\phi - 2L_{11}\sin 2\phi) \tag{1}$$

$$\frac{\mathrm{d}b}{\mathrm{d}t} = -\frac{1}{2}b\left(2L_{11}\cos 2\phi + (L_{12} + L_{21})\sin 2\phi\right) \tag{2}$$

$$\begin{aligned} v_x = \frac{\mathrm{d}x}{\mathrm{d}t} = \frac{1}{4}[&(2L_{11}((1+\mu_r) + (1-\mu_r)\cos 4\phi) + (L_{12}+L_{21})(1-\mu_r)\sin 4\phi)x + (3L_{12} - L_{21} + (L_{12}+L_{21})\mu_r \\ &-(L_{12}+L_{21})(1-\mu_r)(2\cos 2\phi + \cos 4\phi) + 4L_{11}(1-\mu_r)\sin 2\phi + 2L_{11}(1-\mu_r)\sin 4\phi)y] \end{aligned} \tag{3}$$

$$\begin{aligned} v_y = \frac{\mathrm{d}y}{\mathrm{d}t} = \frac{1}{4}[&(3L_{21} - L_{12} + (L_{12}+L_{21})\mu_r - (L_{12}+L_{21})(1-\mu_r)(2\cos 2\phi - \cos 4\phi) + 4L_{11}(1-\mu_r)\sin 2\phi \\ &+2L_{11}(1-\mu_r)\sin 4\phi)x - (2L_{11}((1+\mu_r) + (1-\mu_r)\cos 4\phi) + (L_{12}+L_{21})(1-\mu_r)\sin 4\phi)y] \end{aligned} \tag{4}$$

where ϕ is layer orientation with respect to the fixed axes relative to which the bulk deformation is defined. The velocity gradient tensor can be constructed from the velocities as follows:

$$\mathbf{L} = \begin{pmatrix} \frac{\partial v_x}{\partial x} & \frac{\partial v_x}{\partial y} \\ \frac{\partial v_y}{\partial x} & \frac{\partial v_y}{\partial y} \end{pmatrix} \tag{5}$$

To understand this tensor better in terms of the type of deformation it represents, $\mathbf{L}$ is rotated by $-\phi$ so that it is parallel to the layer and in this reference frame is denoted by $\mathbf{L}'$. Differentiating v_x and v_y appropriately it is found that:

$$\mathbf{L}' = \frac{1}{2}\begin{pmatrix} 2L_{11}\cos 2\phi + (L_{12}+L_{21})\sin 2\phi & L_{12} - L_{21} + (2\mu_r - 1) \times ((L_{12}+L_{21})\cos 2\phi - 2L_{11}\sin 2\phi) \\ -L_{12} + L_{21} + (L_{12}+L_{21}) \times \cos 2\phi - 2L_{11}\sin 2\phi & -2L_{11}\cos 2\phi - (L_{12}+L_{21})\sin 2\phi \end{pmatrix} \tag{6}$$

To understand this tensor it is helpful to decompose it into additive components which add together to make up the above tensor (see for example Lai et al., 1993, p. 108). It can be thought of as being composed of the following deformation components:

$$\mathbf{L}'_{\mathrm{ps}} = \frac{1}{2}\begin{pmatrix} 2L_{11}\cos 2\phi + (L_{12}+L_{21})\sin 2\phi & 0 \\ 0 & -2L_{11}\cos 2\phi - (L_{12}+L_{21})\sin 2\phi \end{pmatrix} \tag{7}$$

representing a pure shear component,

$$\mathbf{L}'_{\mathrm{ss}} = \frac{1}{2}\begin{pmatrix} 0 & 2\mu_r((L_{12}+L_{21})\cos 2\phi - 2L_{11}\sin 2\phi) \\ 0 & 0 \end{pmatrix} \tag{8}$$

representing a simple shear component, and finally

$$\mathbf{L}'_{\mathrm{r}} = \frac{1}{2}\begin{pmatrix} 0 & L_{12} - L_{21} + 2L_{11}\sin 2\phi - (L_{12} + L_{21})\cos 2\phi \\ -(L_{12} - L_{21} + 2L_{11}\sin 2\phi - (L_{12} + L_{21})\cos 2\phi) & 0 \end{pmatrix} \tag{9}$$

representing a pure rotation. The various deformation components are related as follows:

$$\mathbf{L}' = \mathbf{L}'_{\mathrm{ps}} + \mathbf{L}'_{\mathrm{ss}} + \mathbf{L}'_{\mathrm{r}} \tag{10}$$

This analysis corresponds well with the theory of Treagus (1988) in so far as both the pure shear and rotational components of the deformation are independent of the viscosity ratio whereas the simple shear component depends on μ_{r}. Additionally, it demonstrates that for a general bulk two-dimensional deformation the internal deformation of an enclosed layer can be decomposed into layer-parallel pure and simple shear components. The added rotational component corresponds to a rigid rotation and therefore does not affect the final strain state. All three deformation components vary with orientation but only the simple shear component varies with the viscosity ratio.

It is clear from Eq. (6) that the finite strain state resulting from deformation within the layer is due to a continuous superposition of the pure and simple shearing layer-parallel components. In addition, it is important to appreciate that the components of deformation all vary with layer orientation which varies with time as evidenced from both Eqs. (1) and (9). Therefore, because layer orientation varies with time, so too do the deformation components.

The present analysis has important assumptions built into it. As Treagus (1999) highlighted in non-linear materials that viscosity ratio is likely to vary over time and will depend on layer orientation and the bulk deformation history. Therefore viscosity ratio is an effective ratio that describes flow properties integrated over a period of time and that we should really only discuss competence or ductility contrasts (Ramsay, 1982). In the present theory, a Newtonian rheology is assumed and the effect of layer orientation, related variation in layer deformation characteristics and general bulk deformation are considered.

For the remainder of this paper the case of a bulk external pure shear deformation (i.e. $L_{12} = L_{21} = 0$) is considered so that $\mathbf{L}'$ (Eq. (6)) reduces to:

$$\mathbf{L}' = \begin{pmatrix} L_{11}\cos 2\phi & L_{11}(2\mu_{\mathrm{r}} - 1)\sin 2\phi \\ -L_{11}\sin 2\phi & -L_{11}\cos 2\phi \end{pmatrix} \tag{11}$$

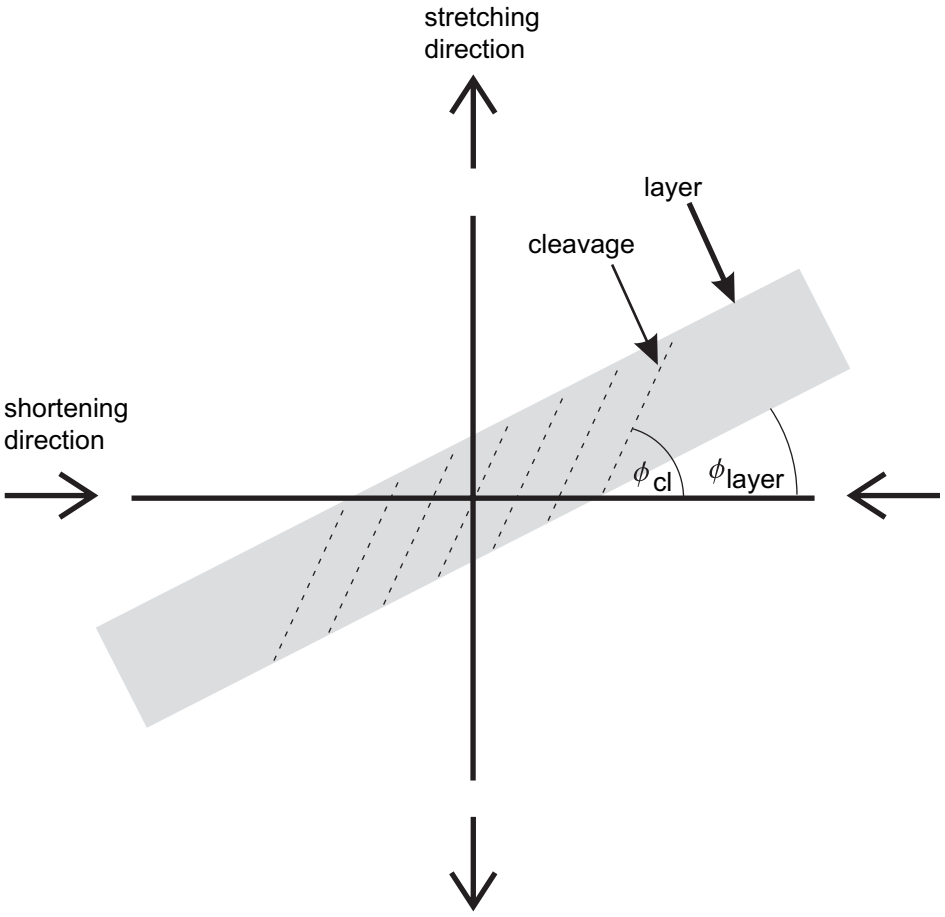

Fig. 1. Schematic representation of situation under consideration. Angles are measured as shown (ϕ_{cl}, cleavage angle and ϕ_{layer}, layer angle).

This choice both simplifies the mathematics and represents a common geological situation where layers are deformed. A schematic representation of the situation is presented in Fig. 1.

2.2. Multilayer

Mulchrone and Walsh (2006) considered the case of an isolated elliptical object of a different viscosity to the surrounding medium. Hence, the present analysis would also appear to only apply to an isolated layer. However, as the long axis of the elliptical object approaches infinity, the disturbed flow usually found near the ellipse disappears and becomes homogeneous and equivalent to the bulk flow. Thus the flow at the layer boundary is equivalent to the bulk flow so that continuity and compatibility is assured for any number of parallel layers. Therefore, the model can also be applied to multilayers.

3. Cleavage refraction, fanning and deformation history

3.1. Introduction

In this section, deformation behaviour is predicted on the basis of kinematic vorticity. This analysis identifies three distinct behavioural categories: (i) less viscous layer ($1 < \mu_r \leq \infty$); (ii) more viscous layer ($(1/2) \leq \mu_r < 1$) and (iii) strongly viscous layer ($0 \leq \mu_r < (1/2)$). Secondly the behaviour of the orientation of the finite strain ellipse and the direction initially normal to the layer (DINL) is investigated for each category.

3.2. Vorticity

Ghosh (1987) showed that in 2D the kinematic vorticity number (W_k) associated with a deformation is calculated from the velocity gradient tensor as follows:

$$W_k = \frac{L_{21} - L_{12}}{\sqrt{L_{11}^2 + L_{22}^2 + (L_{12} + L_{21})^2}} \tag{12}$$

By substituting from Eq. (11), for the present case, W_k is given by:

$$W_k = \frac{L_{11}(\mu_r - 1)\sin 2\phi}{\sqrt{L_{11}^2\left(\cos^2 2\phi + \mu_r^2 \sin^2 2\phi\right)}} \tag{13}$$

If we choose our reference frame such that L_{11} is positive then it cancels out of the expression, giving:

$$W_k = \frac{(\mu_r - 1)\sin 2\phi}{\sqrt{\cos^2 2\phi + \mu_r^2 \sin^2 2\phi}} \tag{14}$$

Differentiating with respect to ϕ and equating to 0, it is found that the minimum and maximum values of W_k occur for $\phi = \pm 45^\circ$. For $\phi = \pm 45^\circ$, we find that:

$$W_k|_{max} = \pm\frac{\mu_r - 1}{\mu_r} \tag{15}$$

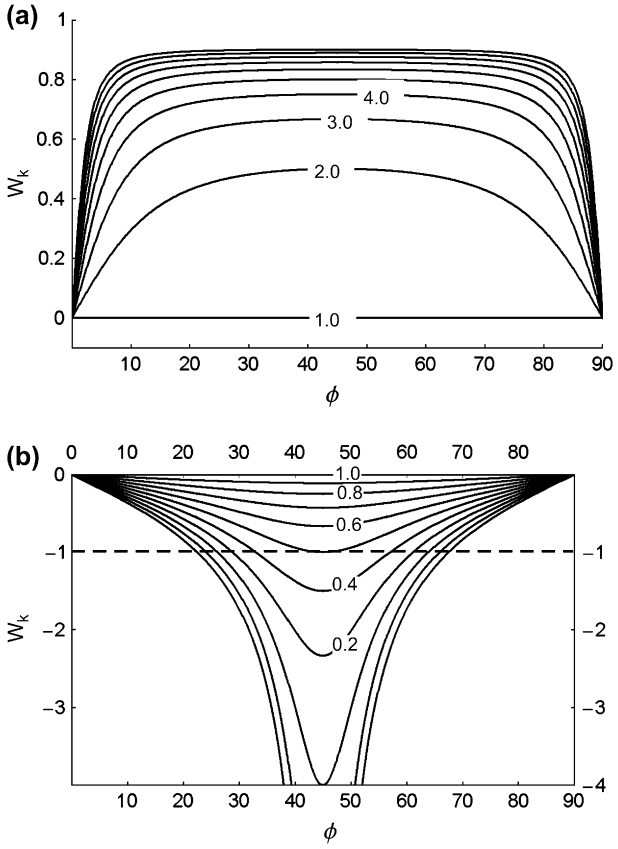

Fig. 2. Variation of vorticity number (W_k) as a function of layer orientation (ϕ) during a bulk pure shear deformation. Numbers annotated on curves represent the viscosity ratio μ_r. (a) Less viscous layer. (b) More viscous layer.

From Eq. (15), it is clear that for less viscous layers ($1 < \mu_r \leq \infty$) the internal layer deformation style can vary from pure shear (i.e. $W_k|_{max} = 0$, $\mu_r = 1$) to an upper limit of simple shear (i.e. $W_k|_{max} = 1$, $\mu_r = \infty$), but that super shear (i.e. $W_k|_{max} > 1$) cannot occur. In Fig. 2 the relationship between μ_r, layer orientation and W_k is illustrated. A tendency exists for the internal layer deformation to rapidly approach simple shear-dominated behaviour even at a relatively small angle to the bulk deformation stretching axes (Fig. 2a). This behaviour is particularly accentuated for layers where $\mu_r > 4$. The shear sense is always antithetic to the rotation of the layer (Fig. 3a).

For more competent layers two classes of behaviour are evident. Firstly, for $(1/2) \leq \mu_r < 1$, the internal deformation ranges from pure shear to simple shear (Fig. 2b) where the shear sense synthetic with the layer rotation (Fig. 3b). For strongly viscous layers, including fully rigid layers ($0 \leq \mu_r < (1/2)$) behaviour ranges from pure to simple shear and beyond into the super shear regime (Ramberg, 1975) as a function of orientation. However, in this case, the angle between the layer and the shortening axis must be in excess of 20°. In other words, for suitably oriented layers whose viscosity is more than twice that of the surrounding medium, super shear and pulsating deformations (Ramberg, 1975) are possible.

It is possible to identify three categories of behaviour according to the model:

- *Type I*: less viscous layer, antithetic.

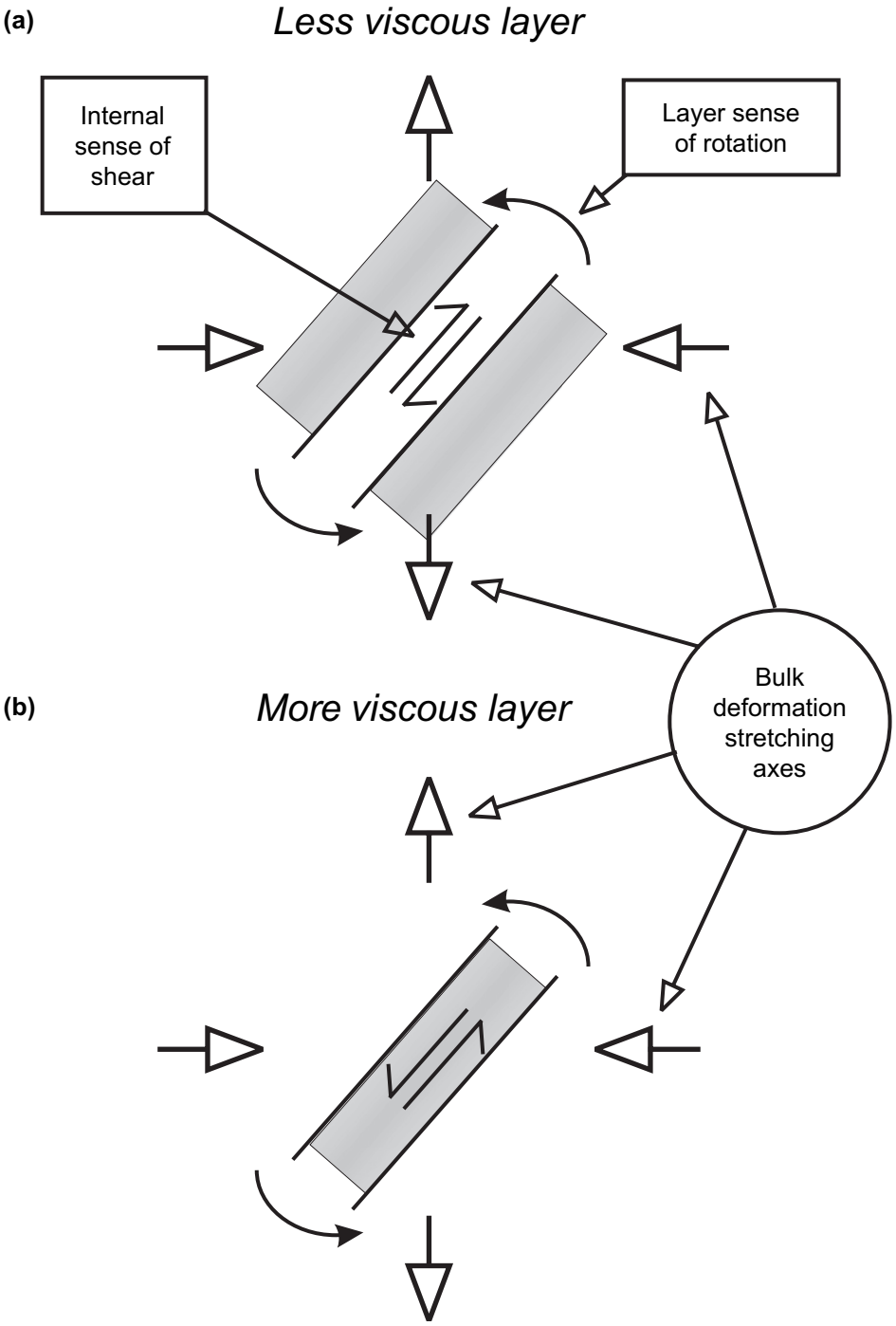

Fig. 3. Sketch illustrating the relationship between layer rotation and internal deformation shear sense.

- *Type II*: more viscous layer, $(1/2) \leq \mu_r < 1$, synthetic.
- *Type III*: strongly viscous layer, $0 \leq \mu_r < (1/2)$, synthetic.

3.3. Finite strain and DINL behaviour

Both the intensity (i.e. axial ratio) and orientation of the finite strain ellipse in a deforming layer are important because cleavage intensity and orientation are assumed to be directly related to finite strain (e.g. Price and Cosgrove, 1990, pp. 450–453). The behaviour of directions initially normal to the layer is also of interest because folding is often interpreted to be preceded by an initial layer-parallel shortening (LPS) with layer-normal cleavage development. This is often true in fold-thrust belts (Mukul and Mitra, 1998, for example).

Provided the layer remains straight, deformation inside the layer is homogeneous at all times so that the evolution of finite strain over time may be calculated using the method given by

Mancktelow (1991) (see also Middleton and Wilcock, 1994, pp. 244–245). To simulate progressive deformation, the layer is initially perturbed to be at a small angle with the shortening direction. This geometry is akin to the approach used in finite-element modelling of buckle fold development whereby an initial sinusoidal perturbation is imparted in a layer to seed fold development (Viola and Mancktelow, 2005). The maximum angle of an initial sinusoidal perturbation can be easily calculated in radians as $(2\pi A/\lambda)$, where A is the amplitude and λ is the wavelength. From a survey of finite-element fold models (see Table 1), it is clear that using layers initially at angles of 2°, 4° and 6° is consistent with common practice. This perturbation is applied to the initial orientation of a perfectly straight layer, which remains a straight layer thereafter, so a sinusoidal perturbation is not used.

Table 1
Perturbation angles employed in previous finite-element studies

Study	Maximum perturbation angle (degrees)
Dieterich and Carter (1969)	3.0
Dieterich and Onat (1969)	20.9
Dieterich (1969)	1.2, 1.5, 3.0
Parrish (1973)	4.0
De Bremaecker and Becker (1978)	20.1, 30.1
Lewis and Williams (1978)	0.05, 0.5, 0.9
Lan and Hudleston (1991)	3.0, 4.0
Mancktelow (1999)	3.0
Viola and Mancktelow (2005)	1.4

Fig. 4 presents the results of the model for a less viscous layer (Type I, $\mu_r = 5.0$), a slightly more viscous layer (Type II, $\mu_r = 0.75$) and a strongly viscous layer (Type III, $\mu_r = 0.2$). For $\mu_r = 0.75$ the DINL orientation and that of the finite strain ellipse are virtually indistinguishable, consistent with the analysis of Treagus (1999). However, for the less viscous layer an initial ($R_s \leq 3.0$) discordance exists of up to 15°. From Fig. 4, it is clear that the layer is rotating counter-clockwise (when counter-clockwise is positive and clockwise is negative) whereas initially the finite strain ellipse is oriented clockwise of the DINL. This result is consistent with the analysis of the previous section. Where $\mu_r = 5.0$, initially both the orientations of the DINL and the finite strain ellipse rotate clockwise whilst the layer rotates counter-clockwise. Depending on the initial layer angle, this rotation changes to counter-clockwise as the layer

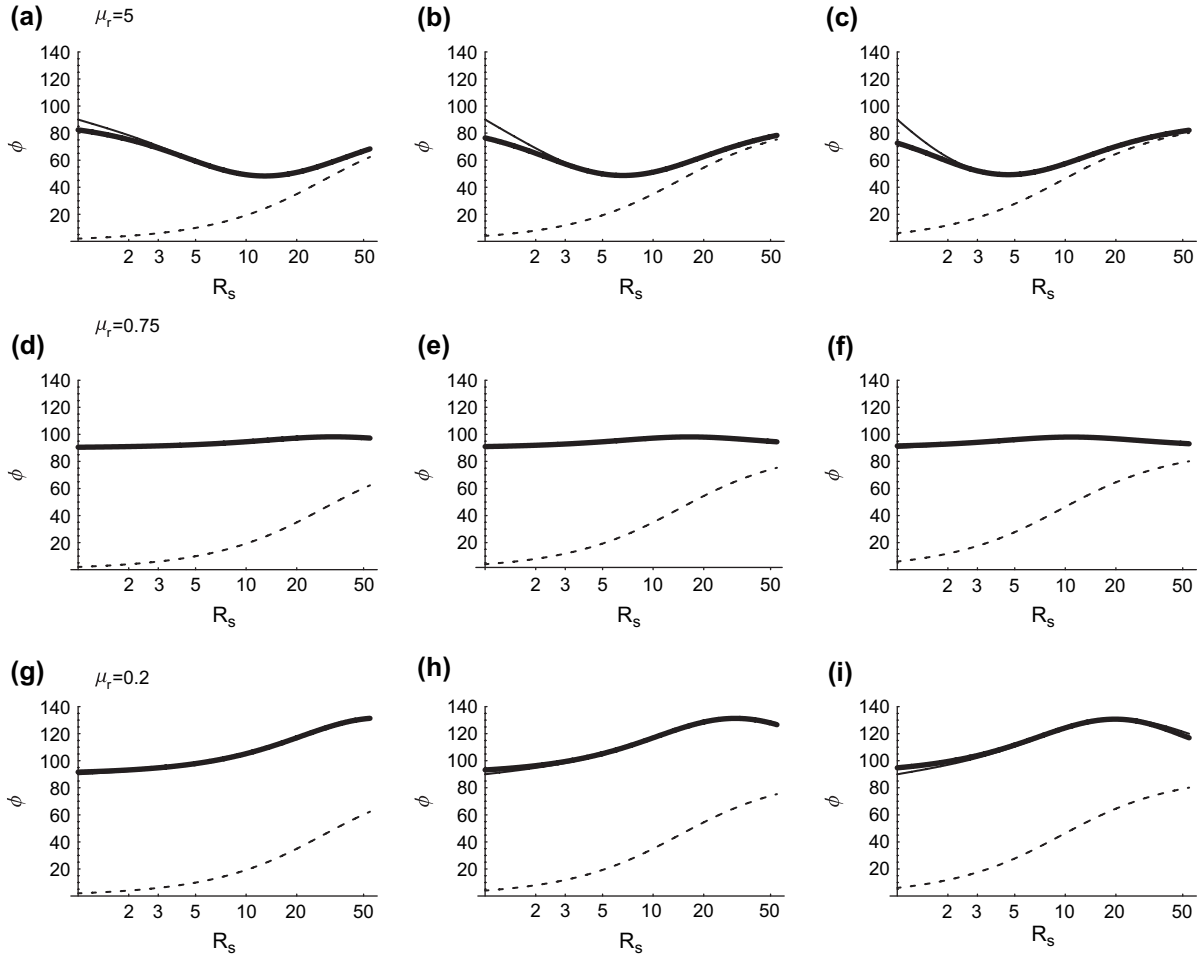

Fig. 4. Graphs illustrating relationships for orientation of layer (dashed line), direction initially normal to the layer (DINL) (medium weight), long axes of strain ellipses (heavy weight) versus the bulk finite strain value (i.e. finite strain axial ratio, R_s). For (a, d, g) the initial layer angle is 2°, for (b, e, h) it is 4°, and for (c, g, i) it is 6°. Note that the ordinate axis is non-linear due to the non-linear accumulation of strain in pure shear with linear time.

steepens to angles in excess of 25°–30°. By contrast, the opposite behaviour occurs for the more viscous layers, where both the finite strain and DINL orientations rotate synthetically with the layer, but once the layer angle exceeds approximately 40° for $\mu_r = 0.75$ and 60° for $\mu_r = 0.2$, they rotate antithetically as layer steepening continues.

Internal deformation accumulates rapidly in the less viscous layer by comparison with the bulk strain, whereas the opposite is true for more viscous layers (Fig. 5). Interestingly for $\mu_r = 0.2$ (a layer only five times more viscous than the surrounding material), the internal deformation unstrains when the bulk shear axial ratio exceeds 18–20, corresponding to layer orientations of around 60°. This unstraining occurs because the long axis of the internal finite strain ellipse rotates along with the layer until it achieves an orientation where the internal deformation essentially reverses the previously accumulated strain. This model clearly illustrates that finite strain values should vary strikingly with lithological and material properties, as well as with deformation history.

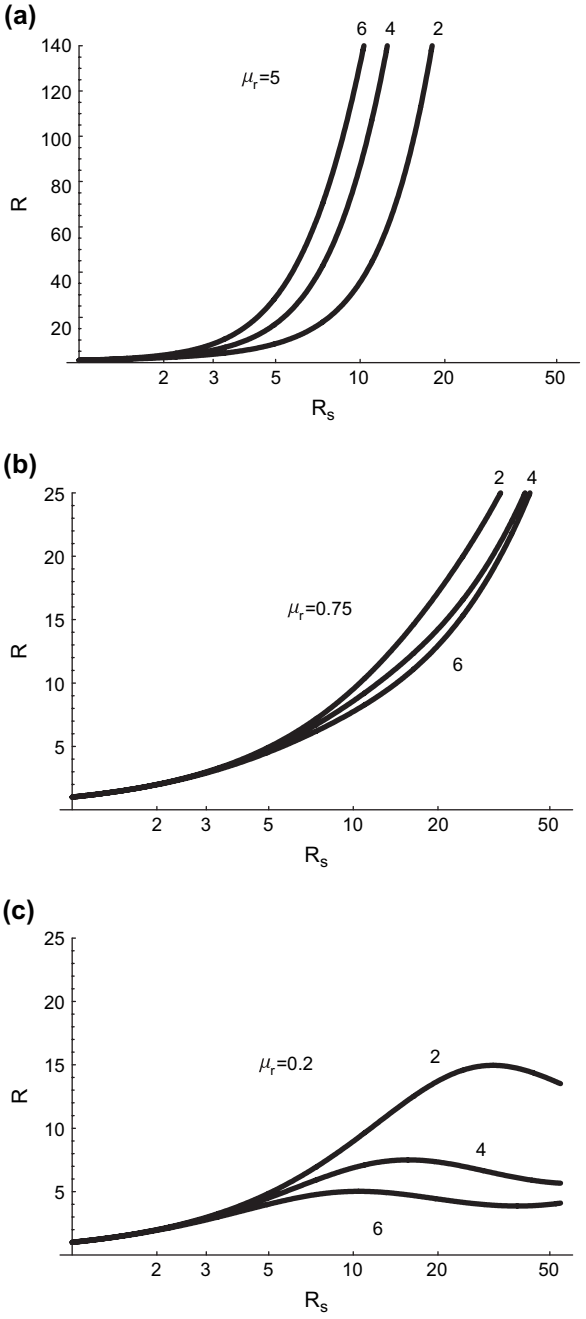

Fig. 5. Graphs illustrating relationship of internal layer finite strain axial ratios (R) versus bulk finite strain (R_s). Numbers adjacent to curves represent the initial orientational perturbation (either 2°, 4° or 6°) given to the layer. Note the varying scales on the y-axis. Note that the ordinate axis is non-linear due to the non-linear accumulation of strain in pure shear with linear time.

4. Application to viscosity ratio determination

4.1. Re-examining the method of Treagus (1999)

Before developing our new method, the method proposed by Treagus (1988, 1999) is examined with data generated by the current model. Treagus (1999) tentatively suggested that at a layer interface the cleavage bedding angles (μ_A and μ_B in Fig. 6, $\mu_r = \mu_B/\mu_A$) can be used to estimate viscosity ratio according to the following relationship:

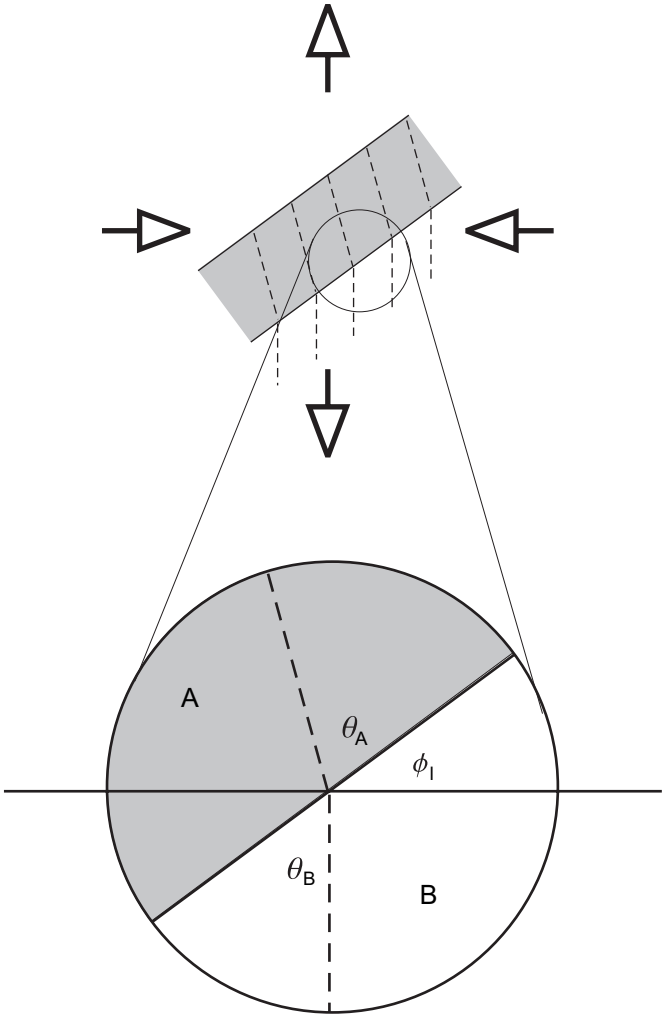

Fig. 6. Cleavage bedding angles used in the method of Treagus (1999). The cleavage bedding angle in layer A is θ_A and for layer B it is θ_B. At any given instance the layer makes an angle ϕ_l with the horizontal. It follows that, $\theta_A = \phi_{sA} - \phi_l$ and $\theta_B = \phi_{sB} - \phi_l$.

$$\frac{\tan\theta_A}{\tan\theta_B} = \frac{\mu_A}{\mu_B} \tag{16}$$

Two representative cases are presented in Fig. 7, with strongly different viscosity ratios were simulated to test the applicability of Eq. (6). For the case of less viscous layer, the initial orientation perturbation of the layer caused a decreasing variation in predicted viscosity ratio and an increasingly accurate prediction with increasing bulk pure shear (Fig. 7a). Conversely, when layer viscosity is 10 times greater than the medium, the accuracy of the predicted viscosity ratio decreases with increasing bulk pure shear while showing greater variation as a function of initial angular perturbation (Fig. 7b). These cases are at opposite extremes. Between them, the method suggested by Treagus (1999) becomes more and more accurate the closer μ_r approaches 1 from either direction. However, outside of these extremes accuracy of estimation decreases.

This analysis shows that the method of Treagus (1999) should lead to fairly accurate estimates of viscosity ratio. It also indicates that estimates from less viscous layers which have not enjoyed much rotation or from steeply oriented competent layers will be less accurate.

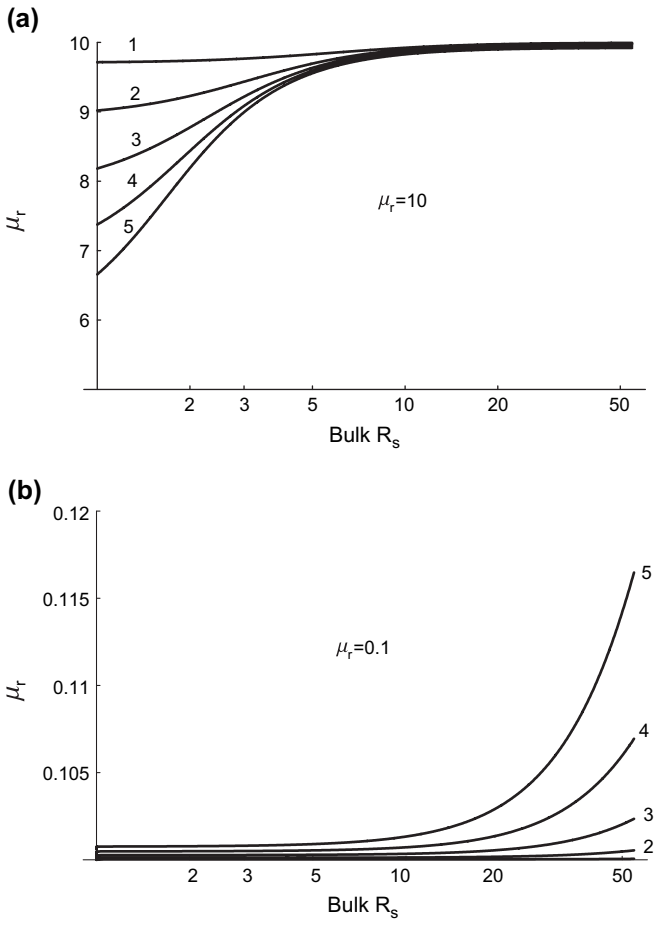

Fig. 7. Plot of estimated μ_r versus bulk strain in the case of an actual value of (a) $\mu_r = 10$ and (b) $\mu_r = 0.1$. The numbers on the curves represent the size of the initial perturbation in degrees. Note that the ordinate axis is non-linear due to the non-linear accumulation of strain in pure shear with linear time.

4.2. Effect of layer-parallel shortening (LPS)

Layer-parallel shortening is suspected to occur in advance of buckling in many geological settings, especially fold-thrust belts (Cooper et al., 1986; Mukul and Mitra, 1998). The effect of such a common deformation behaviour on the determination of viscosity ratio for the method of Treagus (1999) is considered for the case of an LPS with a finite strain magnitude of 2.0. After the LPS, the layer is deformed as before and the method of Treagus (1999) is applied to calculate the viscosity ratio (Fig. 8). Firstly, different initial perturbations in orientation have little effect on the accuracy of the estimation of μ_r, this is why one curve is evident instead of five distinct curves for initial perturbations of 1°, 2°, 3°, 4° and 5°. Secondly and most importantly, we see that the method breaks down badly for small subsequent bulk finite strain; however, it does provide a fairly accurate estimate at high subsequently applied bulk strains. This example illustrates that even though the method of Treagus (1999) works fairly well in the setting of bulk pure shear rotated infinite layers, it must be used with caution in other situations. The added complexity of LPS

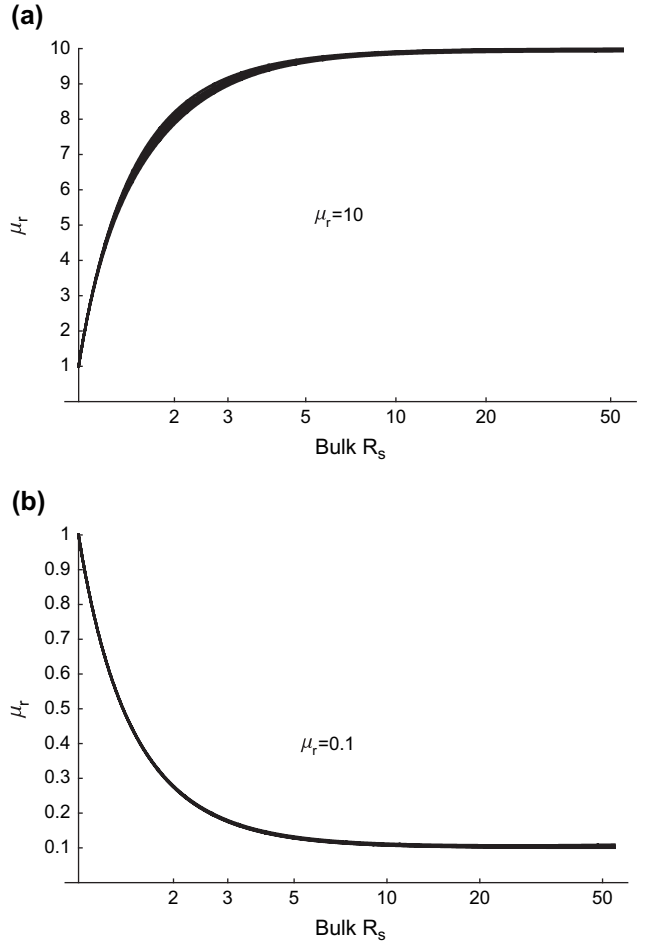

Fig. 8. Plot of estimated μ_r versus subsequently bulk strain in the case of LPS with an actual value of (a) $\mu_r = 10$ and (b) $\mu_r = 0.1$. Curves (overlain and not all visible) represent trajectories for perturbations from 1° to 5°. Note that the ordinate axis is non-linear due to the non-linear accumulation of strain in pure shear with linear time.

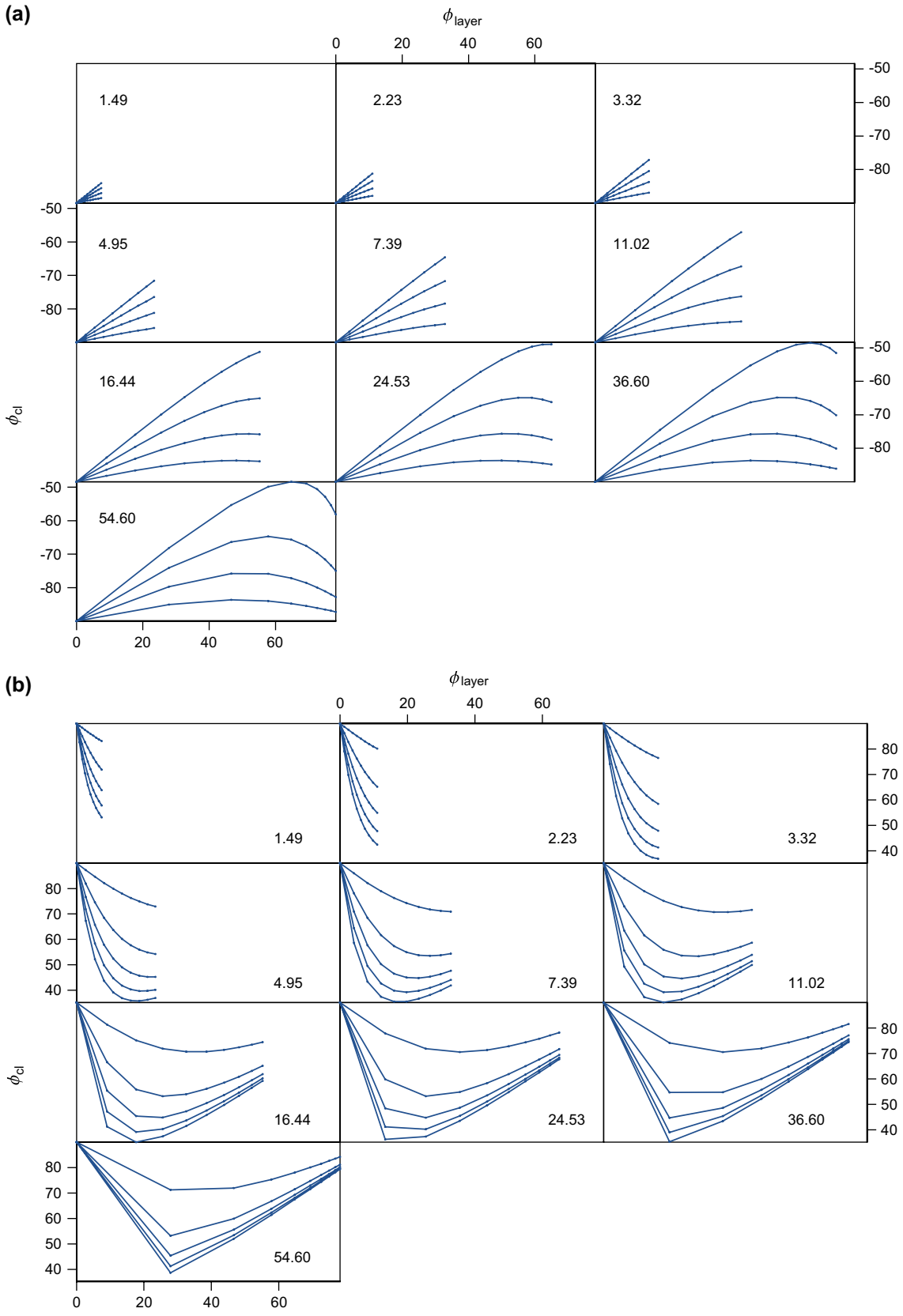

Fig. 9. Cleavage angle (ϕ_{cl}, i.e. finite strain ellipse long axis) versus layer orientation (ϕ_{layer}) for different bulk total strain (value indicated on each graph). See Fig. 1 for definition of angles measured. The series in (a) is for more rigid layers and the values of μ_r are from 0.2 (highest initial slope), 0.4, 0.6 and 0.8 (lowest initial slope). The series in (b) is for less rigid layers and the values of μ_r are from 10 (highest initial slope), 8, 6, 4 and 2 (lowest initial slope).

(and quite likely any deviation from bulk pure shear) may result in erroneous estimates.

4.3. An alternative approach

The previous section naturally leads to an investigation of potential alternative approaches. Perhaps one of the most obvious features of cleavage/strain refraction in the context of a folded layer is the associated fanning of cleavage, commonly observed in the field (Ramsay, 1967, p. 404). Cleavage fanning is related to competency and converges in competent layers whereas it diverges in incompetent layers (Ghosh, 1993, pp. 297–298). On this basis, the relationship between layer and cleavage dip was investigated as a potential candidate for estimating viscosity ratio. Under a bulk pure shear deformation, the variation in limb dip around a fold is due to the ongoing growth of an initial perturbation (Johnson and Fletcher, 1994, pp. 196–218). Therefore, in studying the relationship between limb and cleavage dip, the initial orientation perturbation is varied while the finite strain is constant (Fig. 9).

For each value of μ_r, 10 layers perturbed evenly from 0° to 5° are deformed up to a total bulk strain of 54.60. Layers more viscous than surrounding material have a linear relationship between layer and cleavage dip for strain ratios of up to about 11 (Fig. 9a), implying that cleavage dip is proportional to layer dip. It is also clear from Fig. 9a that the slope of the linear relationship varies with viscosity contrast. As the total strain increases, the relationship between layer and cleavage dip becomes non-linear. It is proposed that by fitting a straight line to layer dip versus cleavage dip data, the slope of the fitted line (slope is used in the mathematical sense and denoted by s) is a suitable measure to compare with μ_r.

The situation for less viscous layers is more complicated (Fig. 9b). A non-linear relationship exists at small strains and a linear relationship emerges only at limb dips $\geq 50°$, which makes simple analysis difficult.

Returning to the case of the more viscous layer ($0 \leq \mu_r < 1$, Types II and III) a graph of the relationship between s and μ_r is given in Fig. 10 for a variety of maximum bulk strains. This graph was produced by varying μ_r from 0 to 1 with 0.01 sized incremental steps as a layer of initial orientation 0.5° evolve. Using the relationship between the cleavage and layer orientation, the value of s was calculated for each value of μ_r. For bulk strains less than approximately 50, the relationship is linear and is simply given by:

$$\mu_r = 1 - s \tag{17}$$

At greater total bulk strains, non-linearities occur, making the relationship difficult to interpret.

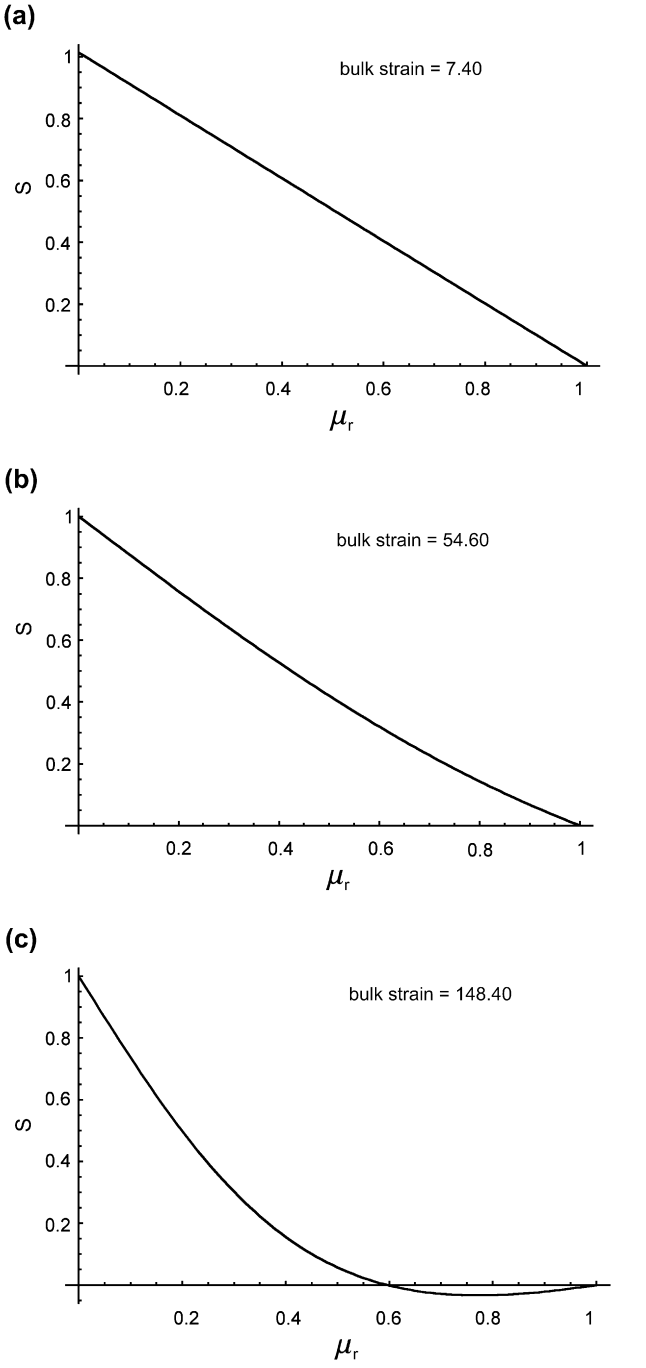

Fig. 10. Graph of the relationship between s and μ_r determined at different total bulk strains. Accumulation of finite strain of 148 is geologically unrealistic but is included here to illustrate that the method becomes unreliable at very high finite strain.

4.3.1. Effect of LPS on the new method

To consider the effect of LPS on the accuracy of the new method, a simulation was performed in Mathematica which varied the component of LPS from 1 to 5 and the total subsequently applied pure shear from 1 to 10. Additionally, the influence of the initial layer perturbation was also investigated. It was found that for small subsequently applied pure shear (i.e. $R_s \leq 2.5$) errors in excess of 10% can occur (Fig. 11). However, if $R_s \geq 5$ then the error is less than 2%. The error does not appear to increase dramatically with the level of LPS and it was found to be independent of the initial layer perturbation. This result contrasts with the strong influence of both layer perturbation and LPS (Fig. 7) on the method tentatively suggested by Treagus (1999).

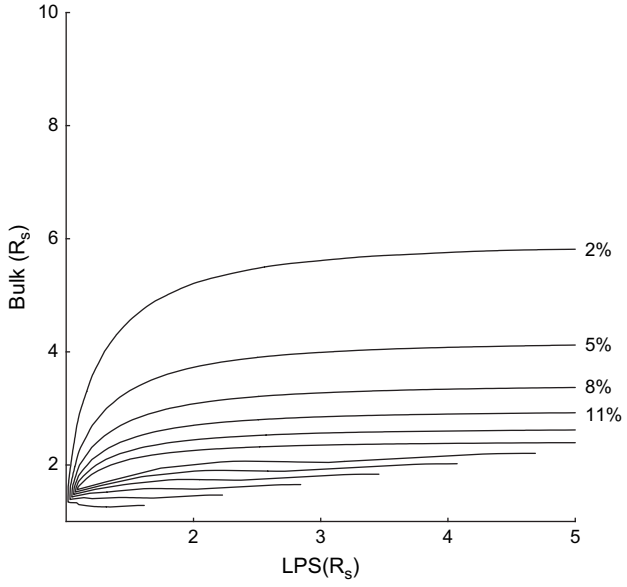

Fig. 11. Graph of error of viscosity ratio estimation as a function of the initial LPS (ordinate axis) and subsequent bulk pure shear (coordinate axis).

5. A case study from the Variscides of southwest Ireland

This study looked at bedding/cleavage relationships across three mesoscopic fold profiles from the Variscan of southern Ireland. This area lies at the western extremity of the Rhenohycernian Zone of the European Variscides and consists of an Upper Palaeozoic, predominantly continental clastic sequence that was deformed into a series of E-W trending regional folds with associated high-angle reverse faultings and penetrative cleavage at the end of the Carboniferous (Gill, 1962; Cooper et al., 1986; Meere, 1995). The first fold is located at White Strand on the Old Head of Kinsale (W 613 428, Irish National Grid), the second at Fountainstown Strand south of the village of Myrtleville (W 788 582) and the third on the southern flank of Hungry Hill on the Beara peninsula (V 745 486). The structure at White Strand consists of well-bedded turbiditic mudstones and medium-grained sandstones of the White Strand Formation (Naylor et al., 1985) folded into an open, steeply inclined and gently plunging anticline with an axial planar cleavage that is best developed in sandstones. In contrast, the fold at Fountainstown contains siltstones of the Kinsale Formation (Naylor, 1966), is again an open, upright, gently plunging anticline with a very well developed penetrative axial planar cleavage. Lastly, the fold at Hungry Hill consists of sandstones and siltstones of the Caha Mountain Formation (Coe and Selwood, 1963) and is also an open, upright, gently plunging anticline with a very well developed axial planar cleavage that is highly penetrative, fine and continuous in the siltstones and more spaced and disjunctive in the sandstones (Fig. 12). For each fold, bedding dip versus cleavage dip is plotted for full fold profiles. The periodicity of the full 180°-dip value range is removed to facilitate the interpretation of the angular relationship between both fabrics (Fig. 13a, b, c).

Data from the Fountainstown fold (Fig. 13a), which consists of a monotonous sequence of siltstones, illustrates that there is negligible cleavage refraction across layers and that the fabric is essentially parallel to the axial plane of the structure. While this geometry is consistent with late-stage cleavage development overprinting the fold, it can also be attributed to early/syn-folding ongoing cleavage development within layers with a low competency contrast as illustrated in Fig. 3d, e, f and Fig. 9b. These plots clearly indicate that in the case of a low competency contrast between units, the orientation of the finite strain ellipse remains remarkably constant with the *x*-axis maintaining a vertical orientation.

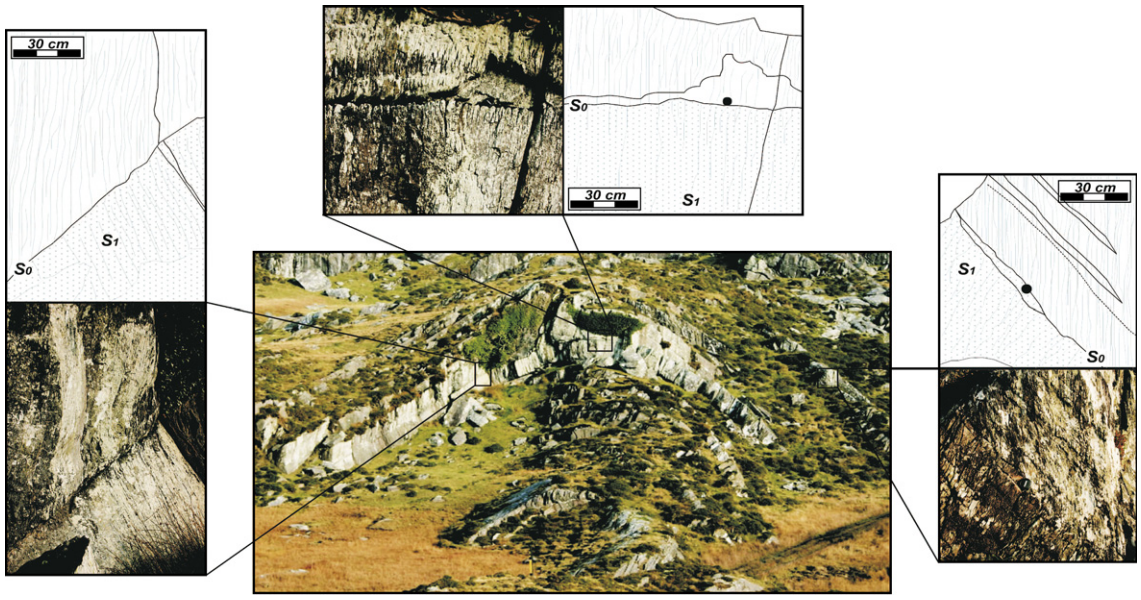

Fig. 12. Field photographs and interpretative sketches of cleavage refraction across the profile of the fold studied on the southern flank of Hungry Hill on the Beara Peninsula, SW Ireland (Irish National Grid: V 745 486). Black lines represent bedding (S_0) and grey lines represent cleavages traces (S_1).

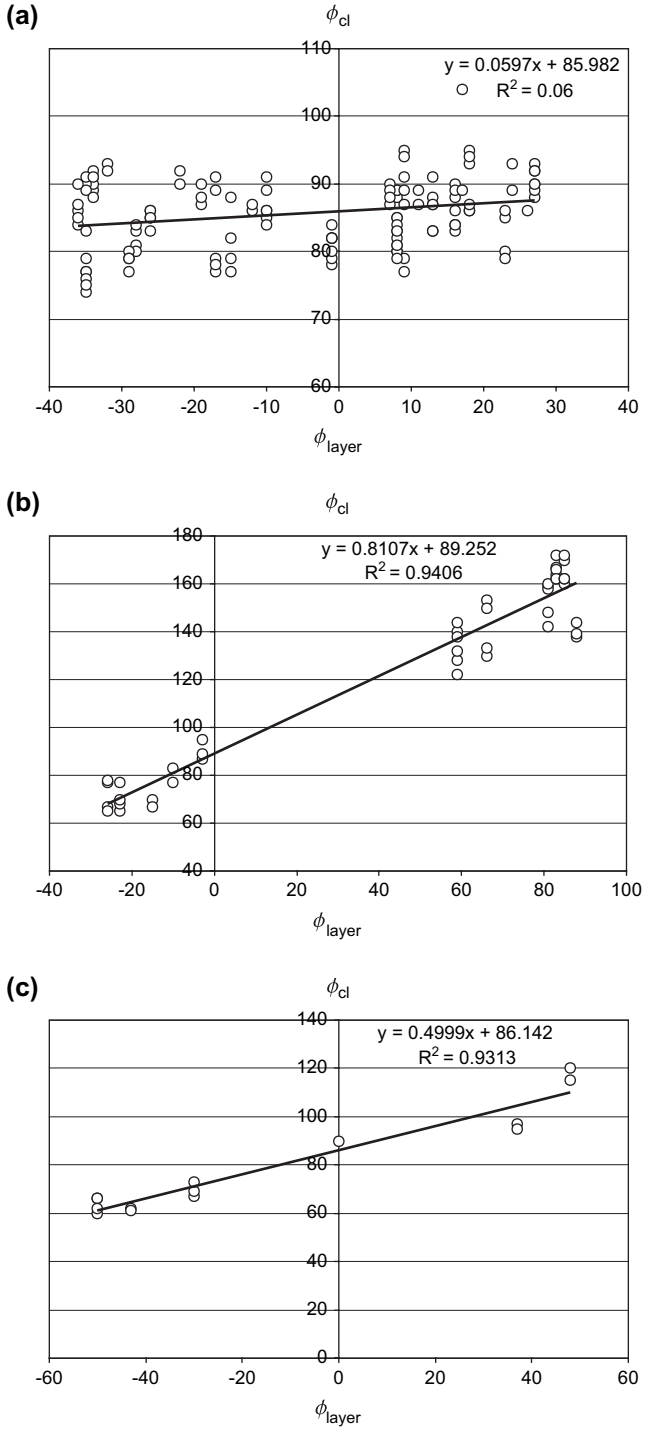

Fig. 13. Plots of fold bedding versus cleavage dip for the three fold profiles studied: (a) Fountainstown; (b) White Strand; and (c) Hungry Hill. The periodicity of the full 180°-dip value range is removed to facilitate the interpretation of the angular relationship between both fabrics.

Data collected from competent sandstone layers in the White Strand fold (Fig. 13b) demonstrate a clear linear relationship between bedding and cleavage dip consistent with the maintenance of high angular discordance between the fabrics during folding as illustrated in Fig. 3g, h, i and Fig. 9a. The slope of the best-fit line between bedding and cleavage is therefore a proxy measure of the competency of this unit. The slope s is estimated to be 0.81, giving a viscosity ratio of 0.19, corresponding to a layer five times more viscous than the surrounding material.

Finally, the data from Hungry Hill (Figs. 12 and 13c) describe cleavage orientation behaviour from interbedded sandstone and siltstone layers. In each case, we see the expected behaviour from both lithologies with cleavage in the less competent siltstones maintaining parallelism with the axial plane while the fabric in the sandstones maintains a high angular discordance with bedding. The slope of 0.50 indicates that the sandstone layer is twice as viscous as the surrounding material. Again, it is evident that this behaviour in bedding/cleavage relationships within units with contrasting competencies across the fold profile cannot uniquely constrain the relative timing of folding and cleavage development. The method of Treagus (1999) was also applied to the fold at Hungry Hill and calculated values for μ_r lie between 0.20 and 0.35, i.e. the sandstone layer is three to five times more viscous than the surrounding material. These estimates are significantly different to the value calculated from the across fold cleavage dip/bedding dip relationship. In view of the linear relationship between cleavage dip and bedding dip (Fig. 13c), it is possible that conditions deviated from the simple bulk pure shear scenario required by Treagus's method. There are a multitude of possibilities including LPS or initiation of cleavage later in the deformation sequence.

Considerable debate has occurred about the relative timing of cleavage development in the Irish Variscan. The prevailing view is that this foreland area enjoyed considerable layer-parallel shortening (LPS) cleavage development prior to the onset of regional buckling and reverse faulting (Cooper et al., 1986; Ford, 1987). Evidence to support LPS includes the parallelism of the XY plane of strain markers (e.g. burrows, desiccation crack septae intersections) to cleavage and the presence of 'sheared cleavage' across bedding planes due to flexural slip folding. The results from this study are a clear illustration that the angular relationship between bedding and cleavage across fold profiles are not a product of a unique folding/cleavage development history and have limited use in establishing a relative deformation chronology between folding and cleavage development. In the case of the Irish Variscan, the parallelism of the XY flattening plane of strain markers with cleavage does therefore not conclusively demonstrate that cleavage development was primarily associated with LPS, and may in fact have been synchronous or even postdate regional folding. The distinction between compositionally sensitive passive cleavage refraction across folded sedimentary layers and simple shear associated with flexural flow folding is also vitally important in constraining the sequence of deformation events in foreland fold/thrust belts. The presence of sheared cleavage is, in itself, not conclusive evidence for early cleavage development as its presence may simply represent a deflection in cleavage dip orientation due to refraction driven by localised competency gradients. This study, therefore, is a clear warning that the importance of LPS in orogenic

forelands, especially in the Irish Variscan, needs to be thoroughly re-examined.

6. Discussion and conclusions

In this paper, we have extended the work of Mulchrone and Walsh (2006) to cover the case of an infinite layer. The layer deformation consists of components of pure shear, simple shear and pure rotation when considered relative to the layer orientation. Concentrating on the case of bulk pure shear, the model allows prediction of the orientation of the long axis of the strain ellipse due to the complex deformation history associated with layer rotation. It was shown how the deformation occurring inside a layer can be vastly different than that of the external (driving) deformation. Using this model, the accuracy of the method for estimating viscosity ratio suggested by Treagus (1999) was tested and found to be reasonably accurate; however, any departure from simple assumptions may lead to erroneous estimates. An alternative approach was developed which relates: (i) the slope of the predicted linear relationship between cleavage dip (i.e. finite strain long axis) and layer dip; and (ii) the viscosity contrast between the layer and the enclosing media. The method only applies in the case of a competent layer and for any fold system where deformation processes do not produce a strain component due to tangential longitudinal strain. It was found that in the case of LPS, the method is robust to deviations from simple scenarios. This robustness is probably due to the use of data from around a fold profile in the method rather than a single sample. The method has been applied to folds from the Irish Variscides which exhibit linear relationships between cleavage and layer orientations. Furthermore, the model indicates that certain features previously used as evidence for LPS in the Irish Variscides are essentially equivocal and cannot be used to argue the case either way.

Acknowledgements

The final version of this paper has been greatly improved by the thoughtful and thorough reviews of Dr. Susan Treagus and Dr. Matty Mookerjee (formerly Strine). We would also like to thank Prof. Bill Dunne for editorial assistance and valuable comments which also helped to improve the final manuscript. This work was supported in part by the Science Foundation Ireland research frontiers programme (grant 04/BR/ES0020).

References

De Bremaecker, J., Becker, E.B., 1978. Finite element models of folding. Tectonophysics 50, 349–367.

Cobbold, P.R., 1983. Kinematic and mechanical discontinuity at a coherent interface. Journal of Structural Geology 5, 341–349.

Coe, K., Selwood, E.B., 1963. The stratigraphy and structure of part of the Beara Peninsula, County Cork. In: Proceedings of the Royal Irish Academy, vol. 63 (section B) 33–59.

Cooper, M.A., Collins, D.A., Ford, M., Murphy, F.X., Trayner, P.M., O'Sullivan, M.J., 1986. Structural evolution of the Irish Variscides. Journal of the Geological Society, London 143, 53–61.

Dieterich, J.H., 1969. Origin of cleavage in sedimentary rocks. American Journal of Science 267, 155–156.

Dieterich, J.H., Carter, N.L., 1969. Stress history of folding. American Journal of Science 267, 129–154.

Dieterich, J.H., Onat, E.T., 1969. Slow finite deformations of viscous solids. Journal of Geophysical Research 74, 2081–2088.

Ford, M., 1987. Practical application of the sequential balancing technique: an example from the Irish Variscides. Journal of the Geological Society, London 144, 885–891.

Ghosh, S.K., 1987. Measure of non-coaxiality. Journal of Structural Geology 9, 111–113.

Ghosh, S.K., 1993. Structural Geology: Fundamentals and Modern Developments. Pergamon Press, Oxford.

Gill, W.D., 1962. The Variscan fold belt in Ireland. In: Coe, K. (Ed.), Some Aspects of the Variscan Fold Belt. Manchester University Press, pp. 49–64.

Harker, A., 1886. On slaty cleavage and allied rock structures with special reference to the mechanical theories of their origin. British Association for the Advancement of Science Report, pp. 813–852.

Johnson, A.M., Fletcher, R.C., 1994. Folding of Viscous Layers: Mechanical Analysis and Interpretation of Structures in Deformed Rock. Columbia University Press, New York.

Lai, W.M., Rubin, D., Krempl, E., 1993. Introduction to Continuum Mechanics, third ed. Butterworth Heinemann Ltd., Oxford.

Lan, L., Hudleston, P.J., 1991. Finite-element models of buckle folds in nonlinear materials. Tectonophysics 199, 1–12.

Lewis, R.W., Williams, J.R., 1978. A finite-element study of fold propagation in a viscous layer. Tectonophysics 44, 263–283.

Mancktelow, N.S., 1991. The analysis of progressive deformation from an inscribed grid. Journal of Structural Geology 13, 859–864.

Mancktelow, N.S., 1999. Finite-element modelling of single-layer folding in elasto-viscous materials: the effect of initial perturbation geometry. Journal of Structural Geology 21, 161–177.

Meere, P.A., 1995. The structural evolution of the western Irish Variscides: an example of obstacle tectonics? Tectonophysics 246, 97–112.

Middleton, G.V., Wilcock, P.R., 1994. Mechanics in the Earth and Environmental Sciences. Cambridge University Press, Cambridge.

Mukul, M., Mitra, G., 1998. Finite strain and strain variation analysis in the Sheeprock Thrust Sheet: an internal thrust sheet in the Provo salient of the Sevier Fold-and-Thrust belt, Central Utah. Journal of Structural Geology 20, 385–405.

Mulchrone, K.F., Walsh, K., 2006. The motion of a non-rigid ellipse in a general 2D deformation. Journal of Structural Geology 28, 392–407.

Naylor, D., 1966. The Upper Devonian and Carboniferous geology of the Old Head of Kinsale, County Cork. Scientific Proceedings of the Royal Dublin Society 15, 229–249.

Naylor, D., Nevill, W.E., Ramsbottom, W.H.C., 1985. Upper Dinantian stratigraphy and faunas of the Old Head of Kinsale and Galley Head, South County Cork. Irish Journal of Earth Science 7, 47–58.

Parrish, D.K., 1973. A nonlinear finite-element fold model. American Journal of Science 273, 318–334.

Price, N.J., Cosgrove, J.W., 1990. Analysis of Geological Structures. Cambridge University Press, Cambridge.

Ramberg, H., 1975. Particle paths, displacement and progressive strain applicable to rocks. Tectonophysics 28, 1–37.

Ramsay, J.G., 1967. Folding and Fracturing of Rocks. McGraw-Hill, London.

Ramsay, J.G., 1982. Rock ductility and its influence on the development of tectonic structures in mountain belts. In: Hsü, K.J. (Ed.), Mountain Building Processes. Academic Press, London, pp. 111–127.

Shimamoto, T., Hara, I., 1976. Geometry and strain distribution of single layer folds. Tectonophysics 30, 1–34.

Siddans, A.W.B., 1972. Slaty cleavage – a review of research since 1815. Earth Science Reviews 8, 205–232.

Sorby, H.C., 1853. On the origin of slaty cleavage. Edinburgh New Philosophical Journal 55, 137–148.

Treagus, S.H., 1973. Buckling stability of a viscous single-layer system, oblique to the principal compression. Tectonophysics 19, 271–289.

Treagus, S.H., 1981. A theory of stress and strain variation in viscous layers, and its geological implications. Tectonophysics 72, 75–103.

Treagus, S.H., 1983. A theory of finite strain variation through contrasting layers and its bearing on cleavage refraction. Journal of Structural Geology 5, 351–368.

Treagus, S.H., 1988. Strain refraction in layered systems. Journal of Structural Geology 10, 517–527.

Treagus, S.H., 1999. Are viscosity ratios of rocks measurable from cleavage refraction? Journal of Structural Geology 21, 895–901.

Viola, G., Mancktelow, N.S., 2005. From XY tracking to buckling: axial plane cleavage fanning and folding during progressive deformation. Journal of Structural Geology 27, 409–417.

Wood, D.S., 1974. Current views on the development of slaty cleavage. Annual Review of Earth and Planetary Sciences 2, 369–401.